International Journal of the Korean Society of Precision Engineering Vol. 4, No. 4, July 2003.

2 Dimensional Modeling of Centerless Grinding - Interference Phenomena -

Kang Kim#

School of Mechanical and Automotive Engineering, Kookmin University, Seoul, South Korea

ABSTRACT

An analytical model of the interference phenomena in the centerless grinding process is developed to investigate their effects on the roundness profile of a centerless ground workpiece. In this work, the regulating wheel and work-rest blade interferences are modeled as a single point contact. The grinding wheel interference is modeled as multiple points contact because material removal is determined by the duration of contact. The computer simulation results show good agreement with the experimental data. From this work, the existence and effects of the interference phenomena in the centerless grinding process are found.

Key Words : Centerless grinding, Interference phenomena

1. Introduction

During centerless grinding, the workpiece is supported by the work-rest blade and regulating wheel, and the material removal is achieved at the contact zone between the workpiece and the grinding wheel. In most theoretical research about the rounding mechanism in centerless grinding,[1-4] it has been assumed that the contact point is fixed at the tangent point of a perfectly round imaginary workpiece. However, in practice, there is a possibility that the real contact points do not coincide with the tangent points because of the irregularity of the workpiece periphery. Rowe[3,5,6] and Barash called this phenomenon "Interference Restriction". They included this restriction in their computer simulation method by applying a clearance condition to modify the apparent depth of cut. Their simulation results showed good agreement with the experimental works in waviness, such as the number of lobes and the relative locations of peaks and valleys. However, details of their simulation results were different from the experimental results. The maximum peak in the simulation is higher than that in the experimental works.

In this paper, mathematical models of interference phenomena at the contact points of the regulating wheel, work-rest blade, and grinding wheel are presented. The workpiece contact points at the regulating wheel and the work-rest blade are assumed as a single point contact. The interference restrictions at the regulating wheel and the work-rest blade are considered to affect only the apparent depth of cut. Because the material is removed at the grinding wheel contact zone, and the duration of contact determines material removal, the grinding wheel contact zone is modeled as multiple points contacts. The interference restriction at this contact zone is analyzed with a machining factor and a machine elasticity factor. The simulation model developed in the previous work[7] is modified to incorporate interference conditions, and the simulation results are compared with the experimental results.

2. Modeling

☞ Manuscript received: February 4, 2003 ;
Accepted: June 18, 2003
Corresponding Author:
Email: kangkim@kookmin.ac.kr
Tel: +82-2-910-4676 ; Fax: +82-2-910-4839

© 2003 KSPE

2.1 Work-rest blade and regulating wheel interference

Fig. 1 shows the configuration of the centerless grinding geometry where θ is the angle of rotation ($\angle O_gOX$) between the initial reference line OX on the workpiece and the grinding wheel contact normal shown as OO_g; α is the angle ($\angle O_gOB$) between the line OO_g and the normal line OB of the work-rest blade surface ; β is the supplementary angle ($\pi - \angle O_gOO_r$) between the line OO_r connecting the workpiece center and the regulating wheel center and the line OO_g; γ is the top angle of the work-rest blade; D_g is the grinding wheel diameter; and D_w is the workpiece diameter. The reference line OX coincides with the line OO_g at the beginning of grinding. The workpiece slides on top of the work-rest blade. Workpiece rotation is governed by the regulation wheel, and the cutting action is performed by the grinding wheel.

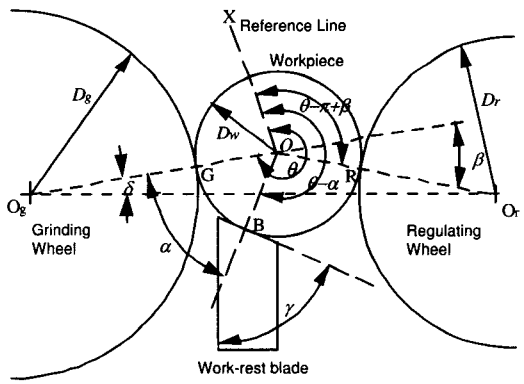

Fig. 1 Centerless grinding geometry

When the irregularities of the workpiece arrive either at the work-rest blade or at the regulating wheel, the workpiece will be displaced, and the apparent depth of cut at the grinding wheel contact point will be changed as shown in Fig. 2, where Δb and Δr are the movements of the workpiece due to the irregularities of the workpiece at the contact points with the work-rest blade and the regulating wheel, respectively.

Fig. 3 shows the schematic diagram of the work-rest blade interference phenomenon. Here $r(\theta)$ is the distance from the reference center, O, in the workpiece to the periphery of the workpiece at angle θ from the reference line OX. It is assumed that the real contact occurs at the workpiece peripheral point of which the normal distance to the workpiece center is the maximum. If the angular displacement difference between this real contact point and the ideal contact point $r(\theta-\alpha)$ is denoted by ζ_θ, the normal distance from the workpiece center to the work-rest blade surface at rotation θ is given as

$$\cos(\zeta_\theta) r(\theta - \alpha + \zeta_\theta) \tag{1}$$

Similarly, at rotation $\theta-\Delta\theta$, the normal distance from the workpiece center to the work-rest blade surface is also described as

$$\cos(\zeta_{\theta-\Delta\theta}) r(\theta - \Delta\theta - \alpha + \zeta_{\theta-\Delta\theta}) \tag{2}$$

Thus, Δb at θ can be expressed as

$$\begin{aligned}\Delta b = &\cos(\zeta_\theta) r(\theta - \alpha + \zeta_\theta) \\ &- \cos(\zeta_{\theta-\Delta\theta}) r(\theta - \Delta\theta - \alpha + \zeta_{\theta-\Delta\theta})\end{aligned} \tag{3}$$

while the workpiece rotates by $\Delta\theta$.

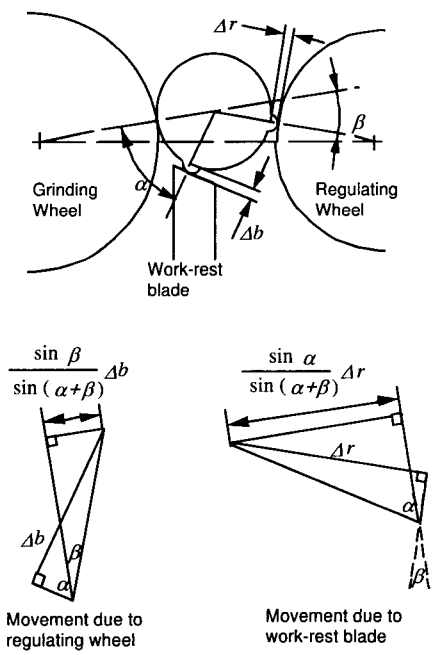

Fig. 2 Movement caused by irregularities at work-rest blade and regulating wheel

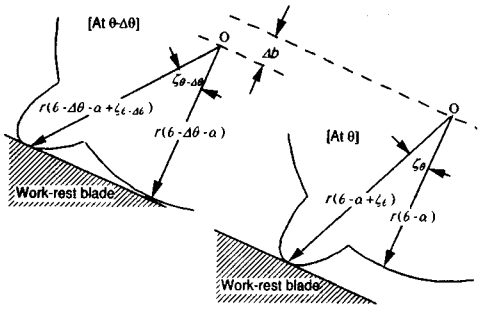

Fig. 3 Work-rest blade interference

A schematic diagram of the interference at regulating wheel contact point is shown in Fig. 4. Normally, the workpiece diameter is much smaller than the regulating wheel diameter. Thus, the regulating wheel surface is considered as a plane which is normal to the line connecting the workpiece center and the regulating wheel center. Under this assumption, the same procedure as the work-rest blade interference model, is used for this regulating wheel interference modeling. If the angular displacement difference between this real contact point at rotation θ and the ideal contact point, $r(\theta-\pi+\beta)$, is ξ_θ, and the angular displacement difference at rotation $\theta-\Delta\theta$ is $\xi_{\theta-\Delta\theta}$, Δr at θ can be expressed as

$$\Delta r = \cos(\xi_\theta) r(\theta - \pi + \beta + \xi_\theta) - \cos(\xi_{\theta-\Delta\theta}) r(\theta - \Delta\theta - \pi + \beta + \xi_{\theta-\Delta\theta}) \quad (4)$$

while the workpiece rotates by $\Delta\theta$.

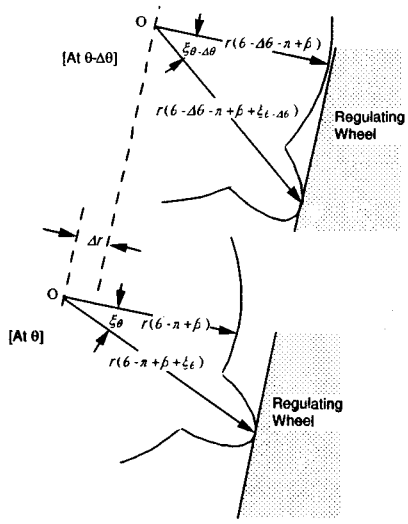

Fig. 4 Regulating wheel interference

The resultant changes in the apparent depth of cut in the grinding wheel contact normal direction are

$$-\frac{\sin\beta}{\sin(\alpha+\beta)}\left\{\cos(\zeta_\theta) r(\theta-\alpha+\zeta_\theta) - \cos(\zeta_{\theta-\Delta\theta}) r(\theta-\Delta\theta-\alpha+\zeta_{\theta-\Delta\theta})\right\} \quad (5)$$

and

$$+\frac{\sin\alpha}{\sin(\alpha+\beta)}\left\{\cos(\xi_\theta) r(\theta-\pi+\beta+\xi_\theta) - \cos(\xi_{\theta-\Delta\theta}) r(\theta-\Delta\theta-\pi+\beta+\xi_{\theta-\Delta\theta})\right\} \quad (6)$$

respectively.

Also, infeed motion increases the apparent depth of cut as shown in Fig. 5. $X(\theta)$ is the magnitude of the infeed motion at θ. Then, the movement of the workpiece in the direction of the grinding wheel contact normal is

$$\cos\delta\left\{X(\theta) - X(\theta-\Delta\theta)\right\} \quad (7)$$

where δ is the angle between infeed motion and grinding wheel contact normal.

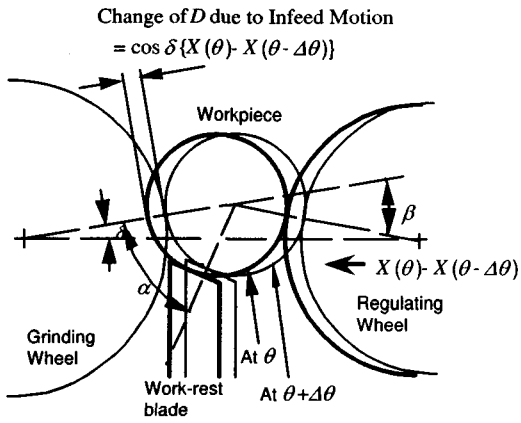

Fig. 5 Change of apparent depth of cut

The instantaneous change in the apparent depth of cut at the grinding wheel contact point can be expressed as the sum of the infeed and the effects of the irregularities at the work-rest blade contact point, regulating wheel contact point, and grinding wheel contact point. Then, the change in the apparent depth of cut, D (θ), in $\Delta\theta$ rotation can be expressed as

$$D(\theta)-D(\theta-\Delta\theta)=\cos\delta\{X(\theta)-X(\theta-\Delta\theta)\}$$
$$-\frac{\sin\beta}{\sin(\alpha+\beta)}\{\cos(\varsigma_\theta)r(\theta-\alpha+\varsigma_\theta)$$
$$-\cos(\varsigma_{\theta-\Delta\theta})r(\theta-\Delta\theta-\alpha+\varsigma_{\theta-\Delta\theta})\}$$
$$+\frac{\sin\alpha}{\sin(\alpha+\beta)}\{\cos(\xi_\theta)r(\theta-\pi+\beta+\xi_\theta)$$
$$-\cos(\xi_{\theta-\Delta\theta})r(\theta-\Delta\theta-\pi+\beta+\xi_{\theta-\Delta\theta})\}$$
$$+\{r(\theta-2\pi)-r(\theta-2\pi-\Delta\theta)\} \quad (8)$$

Similarly,

$$D(\theta-\Delta\theta)-D(\theta-2\Delta\theta)=\cos\delta\{X(\theta-\Delta\theta)-X(\theta-2\Delta\theta)\}$$
$$-\frac{\sin\beta}{\sin(\alpha+\beta)}\{\cos(\varsigma_{\theta-\Delta\theta})r(\theta-\Delta\theta-\alpha+\varsigma_{\theta-\Delta\theta})$$
$$-\cos(\varsigma_{\theta-2\Delta\theta})r(\theta-2\Delta\theta-\alpha+\varsigma_{\theta-2\Delta\theta})\}$$
$$+\frac{\sin\alpha}{\sin(\alpha+\beta)}\{\cos(\xi_{\theta-\Delta\theta})r(\theta-\Delta\theta-\pi+\beta+\xi_{\theta-\Delta\theta})$$
$$-\cos(\xi_{\theta-2\Delta\theta})r(\theta-2\Delta\theta-\pi+\beta+\xi_{\theta-2\Delta\theta})\}$$
$$+\{r(\theta-2\pi-\Delta\theta)-r(\theta-2\pi-2\Delta\theta)\} \quad (9)$$

$$\vdots$$

$$D(\Delta\theta)-D(0)=\cos\delta\{X(\Delta\theta)-X(0)\}$$
$$-\frac{\sin\beta}{\sin(\alpha+\beta)}\{\cos(\varsigma_{\Delta\theta})r(\Delta\theta-\alpha+\varsigma_{\Delta\theta})$$
$$-\cos(\varsigma_0)r(-\alpha+\varsigma_0)\}$$
$$+\frac{\sin\alpha}{\sin(\alpha+\beta)}\{\cos(\xi_{\Delta\theta})r(\Delta\theta-\pi+\beta+\xi_{\Delta\theta})$$
$$-\cos(\xi_0)r(-\pi+\beta+\xi_0)\}$$
$$+\{r(\Delta\theta-2\pi)-r(-2\pi)\} \quad (10)$$

By adding equations (8) through (10), the apparent depth of cut at θ, $D(\theta)$, can be expressed as

$$D(\theta)=D(0)+\cos\delta\{X(\theta)-X(0)\}$$
$$-\frac{\sin\beta}{\sin(\alpha+\beta)}\{\cos(\varsigma_\theta)r(\theta-\alpha+\varsigma_\theta)$$
$$-\cos(\varsigma_0)r(-\alpha+\varsigma_0)\}$$
$$+\frac{\sin\alpha}{\sin(\alpha+\beta)}\{\cos(\xi_\theta)r(\theta-\pi+\beta+\xi_\theta)$$
$$-\cos(\xi_0)r(-\pi+\beta+\xi_0)\}$$
$$+\{r(\theta-2\pi)-r(-2\pi)\} \quad (11)$$

It should be noted that the negative of the last term in equation (11), $\{r(-2\pi)-r(\theta-2\pi)\}$, is the total true depth of cut accumulated at $\theta-2\pi$.

2.2 Grinding wheel interference

Fig. 6 shows the schematic diagram of the grinding wheel interference phenomenon. Normally, the workpiece diameter is also much smaller than the grinding wheel diameter. Thus, the grinding wheel surface is also considered as a plane which is normal to the line connecting the workpiece center and the grinding wheel center. Since material removal is affected by contact duration, the grinding wheel contact zone is modeled as multiple points contact under the grinding wheel interference condition. The apparent depth of cut, $D(\theta)$, is modified as $D(\theta,\eta)$ for each feasible contact point where η is the angle between the ideal contact point and the real contact point. Then,

$$D(\theta,\eta)=D(0,0)+\cos\delta\{X(\theta)-X(0)\}$$
$$-\frac{\sin\beta}{\sin(\alpha+\beta)}\{\cos(\varsigma_\theta)r(\theta-\alpha+\varsigma_\theta)$$
$$-\cos(\varsigma_0)r(-\alpha+\varsigma_0)\}$$
$$+\frac{\sin\alpha}{\sin(\alpha+\beta)}\{\cos(\xi_\theta)r(\theta-\pi+\beta+\xi_\theta)$$
$$-\cos(\xi_0)r(-\pi+\beta+\xi_0)\}$$
$$+\{\cos(\eta)r(\theta+\eta)-r(-2\pi)\} \quad (12)$$

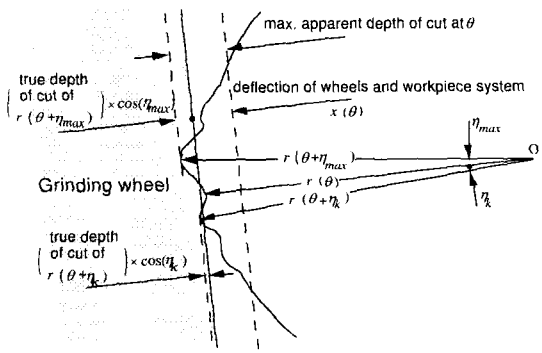

Fig. 6 Grinding wheel interference

To find the deflection of the system, it is assumed that the deflection is initiated at the peripheral point which has the maximum apparent depth of cut, and the grinding wheel surface is always normal to the line connecting the workpiece center and the grinding wheel center. Therefore, the deflection of the system is formulated as a function of the maximum apparent depth of cut. If η_{max} is the angular displacement difference between the point which has the maximum apparent depth of cut, $D(\theta,\eta_{max})$ and the ideal contact point $r(\theta)$, there is the following relationship between the normal grinding force, $F_n(\theta)$ and the deflection of the system, $x(\theta)$:

$$F_n(\theta) = K_e x(\theta) = K_e \cos(\eta_{max}) \{D(\theta, \eta_{max}) - L(\theta, \eta_{max})\} \quad (13)$$

where K_e is the elasticity factor of the machine system and $L(\theta, \eta_{max})$ is the true depth of cut at the point which has the maximum apparent depth of cut.

At this instance, the normal grinding force can also be expressed as

$$F_n(\theta) = K_m \sum_{for\ all\ k} \{\cos(\eta_k) L(\theta, \eta_k)\} + P_0 \quad (14)$$

and

$$L(\theta, \eta_k) = \frac{\cos(\eta_k) D(\theta, \eta_k) - x(\theta)}{\cos(\eta_k)} \quad (15)$$

$$(when\ \cos(\eta_k) D(\theta, \eta_k) \geq x(\theta))$$

where K_m is the machining factor; P_0 is the threshold grinding force; and η_k means η of each real contact point. When $\cos(\eta_k)\ D(\theta, \eta_k)$ is less than the deflection of the system, $x(\theta)$, material removal will be zero. Therefore, if a peripheral point, $r_{old}(\theta + \eta_k)$, is ground at rotation θ, then this peripheral point just after this instantaneous grinding, $r_{new}(\theta + \eta_k)$, can be expressed as

$$r_{new}(\theta + \eta_k) = r_{old}(\theta + \eta_k) - L(\theta, \eta_k) \quad (16)$$

where $L(\theta, \eta_k)$ is the true depth of cut of this peripheral point at this instance.

3. Experiment and Simulation

The experimental details are given in Table 1. The pre-grinding shape of the specimens in this experiment was that of a partially flat cylindrical hollow bar, as shown in Fig. 7. This shape is easy to control and includes all orders of harmonics with the largest amplitudes obtained for the lowest orders. So, it is useful to find any effect of the grinding variables on a certain order of magnitude. The initial roundness error of specimens, except the flat area, was within 2μm, and the depth of flat was 66μm. The roundness profile of the ground specimen as shown in Fig. 8 was measured on the Talyrond 100 machine from Rank Taylor Hobson.

To find the effects of interference phenomena, three different computer simulations were performed under the same grinding condition as shown in Table 1. The first

Table 1 Experimental condition

Grinding machine	Cincinnati CINCO 15
Grinding Wheel	97A 80 J6 VFM ϕ584.2 × 101.6 × 304.8 mm hole
Regulating Wheel	A80 R2 ϕ322.5 × 101.6 × 127.0 mm hole
Work-rest blade	Sintered Carbide
Specimen	Steel (H_{RC} = 62)
Geometric set-up	α = 57.9°, β = 5.9°, γ = 60°
R.W. speed G.W. speed	20 rpm 1200 rpm
Total infeed Infeed time	77 μm 7.5 sec equivalent to 35 rev. of workpiece
Spark out time	6.0 sec equivalent to 28 rev. of workpiece
Dressing traverse rate	53 μm/rev. (2.5"/min) (4 passes 25.4 μm (0.001") depth)

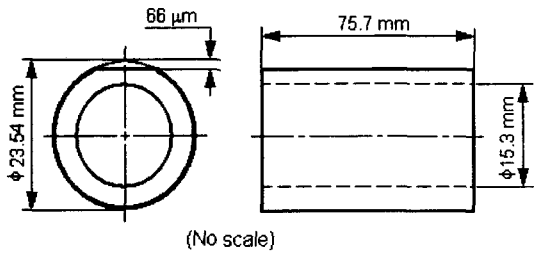

Fig. 7 Before-grinding shape of specimen

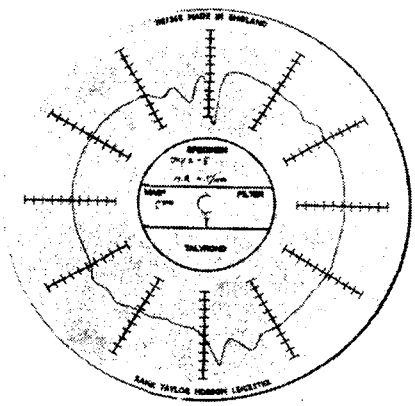

Fig. 8 Experimental result (1 scale = 5μm)

simulation was done using the model without the interference restrictions. The second one used the model including the work-rest blade and regulating wheel interference restrictions. The grinding wheel interference restriction was added for the last one.

In the simulations, the workpiece was divided into

360 equi-spaced radii. The magnitude of these radii at any given moment defined the shape of the workpiece. The initial contact point between the workpiece and grinding wheel was determined by finding the maximum displacement at the grinding wheel contact in one revolution using the following equation:

$$MAX\left[-\frac{\sin\beta}{\sin(\alpha+\beta)}r(\phi-\theta)+\frac{\sin\alpha}{\sin(\alpha+\beta)}r(\phi-\pi+\beta)+r(\phi-2\pi)\right]$$

$$(0\le\phi\le 2\pi) \qquad (17)$$

The workpiece was rotated in steps of 1°. The corresponding angular range of the initial flat width was ±7°. Thus, the peripheral points within the ranges $\theta-\alpha\pm7°$ and $\theta-\pi+\beta\pm7°$ were checked at every θ to find the true contact points in the work-rest blade and the regulating wheel interference models. In the same way, the peripheral points within the ranges $\theta\pm7°$ were considered as feasible grinding wheel contact points.

For this interference model, the threshold grinding force, P_0, 210N, was quoted from the reference 8, and the machining factor, K_m, was calculated as 195.5MN/m from the empirical equation in the reference 7. The elasticity factor, K_e, 20MN/m, was cited from the reference 9.

4. Discussions

All the simulation results in Fig. 9 show that the number of lobes and the angular displacement of peaks and corresponding valleys are similar to what are shown in the experimental result. The simulation result of the first model without interference restrictions, (Fig. 9-a), shows that the roundness profile was directly governed by the 'equi-diametral control rule'. In this case, there was no big difference between the height of the maximum peak (31μm) and the depth of the maximum valley (34μm). But the corresponding values in the experimental work (Fig. 8) were 20μm and 30μm, respectively.

This maximum peak error caused the depth error of a maximum valley in the simulation results, and this trend was propagated to the next peak and valley. Also, the peaks of this simulation result were duller and thicker than those of the experimental work.

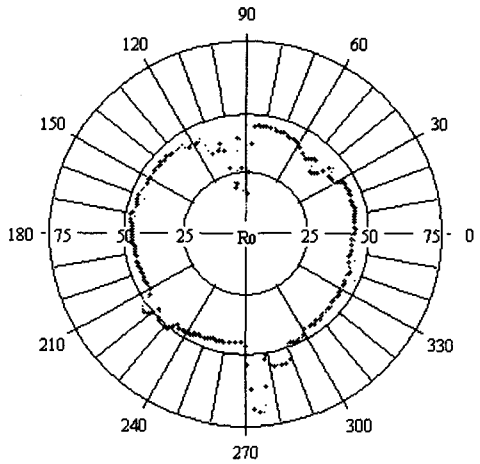

a) no interference

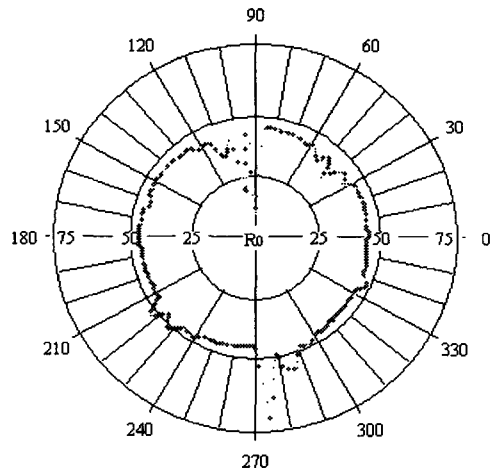

b) work-rest blade & regulating wheel interference

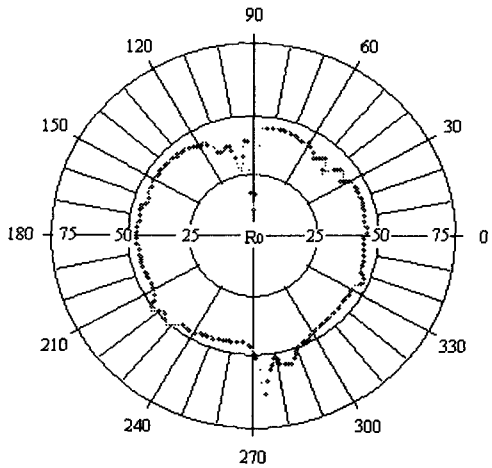

c) work-rest blade, regulating and grinding wheel interference

Fig. 9 Simulation results (Unit: μm)

Fig. 9-b shows the simulation result of the second model using the work-rest blade and regulating wheel interference restrictions. The height of the peak still shows a big difference from that of the experimental work. Accordingly, the error propagation can also be found in this simulation result. But, in this model, it can be expected that the apparent depth of cut is greater than that of the first model in the vicinity of peaks or valleys. Therefore, the true depth of cut is also greater than that of the first model around these points. So the peaks were sharper and thinner than those of the first simulation result.

The simulation result of the third model, including the grinding interference restriction to the second model, is shown in Fig 9-c. Under this restriction, the points around the peak are ground longer in each revolution of the workpiece. Therefore, these points can be ground more without any effect on the points around the maximum valley. The simulation result shows that the height of the maximum peak was reduced from 31μm to 21μm. As a result of this reduction, the error at the second maximum valley was also cleared, and this error correction propagated all over the workpiece periphery. The model matched well with the centerless infeed grinding process not only in global shape generation but also in the details of the rounding mechanism.

5. Conclusions

An analytical simulation model of the interference phenomena in the centerless grinding process was developed to investigate these effects on the roundness profile of a centerless ground workpiece. The regulating wheel and work-rest blade interferences were modeled as a single point contact. It was found that the width of the peaks and valleys was sharper and thinner from the effects of these interferences. The grinding wheel interference was modeled as multiple points contact. This model included the concept of the machining elasticity. It was also found that the height of the peaks and the depth of the valleys in the simulation approached the corresponding experimental result by applying the grinding wheel interference model. From this work, the existence and effects of the interference phenomena in the centerless grinding process were found.

References

1. Dall, A. H., "Rounding Effect in Centerless Grinding," Mech. Engg, Vol. 68, No. 4, pp. 325-329, Apr. 1946.
2. Yonetsu, S., "Forming Mechanism of Cylindrical Work in Centerless Grinding," Proc. Fujihara Memorial Faculty of Engineering, Keio Univ., Vol. 12, No. 47, pp. 27-45, 1959.
3. Rowe, W. B. and Barash, M. M., "Computer Method for Investigating the Inherent Accuracy of Centerless Grinding," Int. J. MTDR, Vol. 4, No. 2, pp. 91-116, 1964.
4. Chien, A. Y., "The Rounding off Theory of Centerless Grinding," Int. J. MTDR, Vol. 21, No. 1, pp. 49-55, 1981.
5. Rowe, W. B., Miyashita, M. and Koenig, W., "Centerless Grinding Research and its Application in Advanced Manufacturing Technology," Annals of CIRP, Vol. 38, pp. 617-625, 1989.
6. Rowe, W. B., Barash, M. M. and Koenigsberger, F., "Some Roundness Characteristics of Centerless Grinding," Int. J. MTDR, Vol. 5, No. 4, pp. 203-215, 1965.
7. Kim, K., Chu, C. N. and Barash, M. M., "Roundness Generation during Centerless Infeed Grinding," Trans. of NAMRI, Vol. 20, pp. 167-172, May 1992.
8. ASM International, Metals Handbook, 9th ed., Vol. 16 Machining, pp. 422, 1989.
9. Reshetov, D. N. and Portman, V. T., Accuracy of Machine Tools, ASME Press, pp. 275, 1988.